Secondary fluorescence in electron probe microanalysis of material couples

X Llovet[1], P T Pinard[2], J J Donovan[3] and F Salvat[4]

[1] Centres Científics i Tecnològics, Universitat de Barcelona. Lluís Solé i Sabarís, 1-3, 08028 Barcelona, Spain
[2] Gemeinschaftslabor für Elektronenmikroskopie, RWTH Aachen. Ahornstrasse 55, 52074 Aachen, Germany
[3] CAMCOR, Department of Chemistry, University of Oregon. Eugene, OR 97403, USA
[4] Facultat de Física (ECM and ICC), Universitat de Barcelona. Diagonal 647, 08028 Barcelona, Spain

E-mail: xavier@ccit.ub.edu

Abstract
We describe a semi-analytical method for the fast calculation of secondary fluorescence in electron probe microanalysis of material couples. The calculation includes contributions from primary K-, L- and M-shell characteristic x-rays and bremsstrahlung photons. The required physical interaction parameters (subshell partial cross sections, attenuation coefficients, etc) are extracted from the database of the Monte Carlo simulation code system PENELOPE. The calculation makes use of the intensities of primary photons released in interactions of beam electrons and secondary electrons. Since these intensities are not readily available and do not allow analytical calculation, they are generated from short Monte Carlo simulation runs. The reliability of the proposed calculation method has been assessed by comparing calculated, distance-dependent k-ratios with experimental data available in the literature and with results from simulations with PENELOPE. Numerical results are found to be in close agreement with both simulated and experimental data.

(Some figures may appear in colour only in the online journal)

1. Introduction

Electron probe microanalysis (EPMA) is a widely used technique for material analysis. Quantitative analysis is obtained by measuring the energy spectra of x-rays emitted from the specimen under irradiation with a focused electron beam. Typically, the energy of the electron beam ranges from a few keV up to about 50 keV. This paper describes simple models for the fast calculation of approximate secondary fluorescence corrections in EPMA, which are required for converting measured x-ray intensities into element concentrations. Although the effective electron range is relatively small (of the order of a few μm), characteristic primary x-rays penetrate much deeper into the specimen and can ionize atoms at much larger distances, thus degrading the spatial resolution of the technique as well as the accuracy of evaluated chemical compositions (Reed and Long 1963). Analytical formulae to account for secondary fluorescence corrections in simple geometries have been proposed for homogeneous specimens (Reed 1965), for material couples (Hénoc et al 1969, Maurice et al 1965, Bastin et al 1983), for thin films on substrates (Cox et al 1979) and for multilayers (Youhua et al 1988). Usually, these formulae only account for fluorescence from characteristic x-rays, the contribution from the bremsstrahlung continuum has only been considered for homogeneous samples. In this work we describe a semi-analytical method for the fast calculation of secondary fluorescence for homogeneous samples and material couples, including characteristic and continuum fluorescence. Preliminary results have been presented elsewhere (Escuder et al 2010).

In the theoretical analysis and calculations that follow, we use the physical interaction models implemented in the general-purpose Monte Carlo code system PENELOPE (Salvat et al 2009). This code provides a realistic description of the elementary interactions of electrons and photons, which combines elaborate analytical models with extensive numerical databases. The subshell partial cross

sections, attenuation coefficients, etc employed in the present calculations are extracted from the PENELOPE database. Quantities that do not allow an analytical calculation are obtained from short runs of the Monte Carlo simulation code, using a dedicated main program that automatically generates all the required quantities and parameters. Simulations of EPMA experiments are performed using the main program PENEPMA (Llovet *et al* 2005, Salvat *et al* 2009), which has been employed previously to describe fluorescence corrections (Llovet and Galan 2003, Fournelle *et al* 2005).

We assume the usual geometrical arrangement of EPMA measurements, i.e. a parallel beam of electrons with kinetic energy E_0 impinging normally on the flat surface of a specimen. As a result of the interactions of the beam (primary) electrons *and* of the secondary radiation generated within the specimen, characteristic and bremsstrahlung photons emerge from the specimen surface. These photons are recorded by a detector that subtends a small solid angle in a direction that makes an angle θ_d with the outgoing normal to the surface of the specimen. The information required for the quantitative analysis of the active volume of the specimen is provided by the intensities of characteristic lines in the recorded spectrum.

2. Photon emission from a homogeneous specimen

Let us start by considering the case of EPMA measurements on homogeneous specimens. In the course of their walk within the specimen, primary electrons (i.e. those of the incident beam) may undergo hard inelastic interactions in which fast secondary electrons are released. These secondary electrons can also cause the emission of photons by impact ionization of inner atomic electron shells and by bremsstrahlung emission. In the former case, the residual ion with a vacancy in the active inner shell relaxes to the atomic ground state through a cascade of radiative and nonradiative transitions and emits x-rays and Auger electrons with discrete characteristic energies. Bremsstrahlung photons have a continuous energy distribution, which extends up to the energy E_0 of the electron beam. Photons emitted by primary electrons *and* by fast secondary electrons will be qualified as primary photons.

While characteristic x-rays (and Auger electrons) are emitted isotropically, bremsstrahlung quanta have initial directions that are correlated with the direction of the radiating electron. Nevertheless, as the direction of motion of electrons in a solid becomes rapidly randomized by elastic (and inelastic) collisions, primary bremsstrahlung photons have a broad angular distribution. For the sake of simplicity, we will assume that all primary photons are emitted isotropically.

Primary photons can, in turn, interact with the specimen, primarily through the photoelectric effect and Compton scattering. Hence, photons emitted originally in the direction of the detector may be absorbed within the specimen (absorption effect). Furthermore, interactions of primary photons may cause the ionization of inner shells of atoms, which relax to their ground state by emitting secondary characteristic x-rays (fluorescence) and Auger electrons. Fluorescence caused by characteristic x-rays and bremsstrahlung photons will be referred to as characteristic

fluorescence and bremsstrahlung fluorescence, respectively. In turn, secondary radiations may interact and produce third-generation radiations, and so on. In practice, the contribution to the measured spectrum of photons from the third and higher generations is very small and can be neglected.

A material M described by means of its chemical formula, $(Z_1)_{n_1} (Z_2)_{n_2} \ldots$, is considered, where $Z_1, Z_2, \ldots$ are the atomic numbers of the elements present, and $n_1, n_2, \ldots$ are the corresponding stoichiometric indices. In the case of compounds, n_a is the number of atoms of element Z_a in a molecule; the molar mass (g mol^{-1}) is $A_{\text{mol}} = n_1 A_{\text{w}}(Z_1) + n_2 A_{\text{w}}(Z_2) + \cdots$, where $A_{\text{w}}(Z_a)$ is the atomic weight of the element Z_a. For mixtures and alloys, the numerical values of the stoichiometric indices are proportional to the percentage number of atoms, p_a, of each element. That is, $n_a = C p_a$, where C is a positive number; the value of C defines the size of a 'molecule'. Of course, a 'molecule' will usually contain fractions of atoms, but this is not a source of conflict provided we define the molecular cross section as the properly weighted sum of atomic cross sections. The number of molecules per unit volume is

$$\mathcal{N} = \frac{N_{\text{A}}\rho}{A_{\text{mol}}}, \tag{1}$$

where N_{A} is Avogadro's number and ρ is the mass density of the material (in g cm^{-3}). The number of atoms of the element Z_a per unit volume is

$$\mathcal{N}_a = n_a \mathcal{N} = c_a \frac{N_{\text{A}}\rho}{A_{\text{w}}(Z_a)} \tag{2}$$

where

$$c_a = \frac{n_a A_{\text{w}}(Z_a)}{A_{\text{mol}}} \tag{3}$$

is the mass fraction of the element Z_a.

2.1. Intensities of primary photons

The first ingredient for the calculation of fluorescence corrections is the intensity of the primary photons, that is, the number of primary photons that are emitted per unit solid angle. Evidently, this intensity depends on the energy E_0 of the electron beam (and on the direction of incidence). In general, accurate intensities of primary photons can only be calculated from Monte Carlo simulations.

A rough approximation for the intensity of primary photons may be obtained by neglecting backscattering effects (electrons that are backscattered from the specimen do not generate photons) and using the continuous slowing down approximation (CSDA) to describe the stopping of electrons in matter. The CSDA assumes that electrons of energy E lose energy continuously; the energy loss per unit path length is given by the stopping power $S(E) = -\text{d}E/\text{d}s$. Thus, the intensity $I_1(E_1)$ of primary characteristic x-rays of energy E_1 released by atoms of the element Z_a in the filling of a subshell i by electrons from an outer subshell can be obtained as

$$I_{\text{M}}(E_0, E_1) = \frac{P_{i,1}}{4\pi} \mathcal{N}_a \int_{E_i^{\text{ion}}}^{E_0} \sigma_i(E) \frac{\text{d}E}{S(E)}, \tag{4}$$

where $\sigma_i(E)$ is the cross section for the production of a vacancy in the ith subshell of the target atom by impact electrons with kinetic energy E, E_i^{ion} is the ionization energy of that subshell, and $P_{i,1}$ is the probability that the vacancy in subshell i is filled through the radiative transition that releases the characteristic photon of energy E_1. Note that the vacancy in the active shell can be the result of either the direct impact ionization of that shell or of the relaxation of vacancies generated by impact ionization of deeper shells (with ionization energies larger than E_i^{ion}). The product $\mathcal{N}_a \sigma_i$ is the electron's inverse mean free path for the production of a vacancy in the active subshell (i.e. the mean number of i-shell vacancies generated per unit path length). Similarly, the intensity of bremsstrahlung quanta (number of photons emitted per unit photon energy and unit solid angle, assuming isotropic emission) can be evaluated as

$$\frac{\mathrm{d}I_{\mathrm{br,M}}(E_0, E_1)}{\mathrm{d}E_1} = \frac{1}{4\pi}\mathcal{N} \int_{E_1}^{E_0} \frac{\mathrm{d}\sigma_{\mathrm{br}}(E)}{\mathrm{d}E_1} \frac{\mathrm{d}E}{S(E)}, \qquad (5)$$

where $\mathrm{d}\sigma_{\mathrm{br}}(E_0)/\mathrm{d}E_1$ is the molecular differential cross section for emission of bremsstrahlung photons of energy E_1 by electrons of energy E_0 in material M. Hereafter, quantities pertaining to primary photons will be denoted by the subscript 1.

Although expressions (4) and (5) can be calculated fairly easily, it is more expedient to obtain the intensities from Monte Carlo simulations. As indicated above, we use the Monte Carlo code system PENELOPE (Salvat *et al* 2011) which implements the most accurate interaction models available, limited only by the required general features of the code, a tunable simulation scheme for tracking electrons (and positrons), and an efficient geometry package. Electron histories are generated using a mixed simulation algorithm: electron hard interactions (involving energy transfers or angular deflections larger than certain cut-off values) are simulated individually from the corresponding differential cross sections, while the effect of soft interactions (involving energy transfers and angular deflections smaller than the corresponding cut-offs) is described using multiple scattering approximations. Photon histories are generated using the conventional detailed scheme, in which interactions are simulated individually in chronological order. X-ray spectra from targets irradiated by electron beams are generated using the dedicated main program PENEPMA (Pinard *et al* 2012). To improve the efficiency of the simulation, PENEPMA makes use of the variance-reduction technique of interaction forcing for inner-shell ionization and bremsstrahlung emission events. In particular, this technique consists of artificially increasing the probability of occurrence of the processes of interest (i.e. those ending with the emission of photons) and assigning appropriate statistical weights to the generated photons in order to keep the simulation results unbiased.

Using the program PENEPMA, we can evaluate intensities of primary photons from homogeneous specimens as functions of the energy E_0 of the incident electron beam. The simulation for each beam energy takes minutes on a single processor, so that primary intensities can be routinely calculated for each desired material. We have found that these intensities are closely reproduced by simple analytical expressions, with parameters determined by least-squares fittings to Monte Carlo data. Thus, the intensity of primary characteristic x-rays can be expressed as a polynomial in $E - E_i^{\mathrm{ion}}$, where E_i^{ion} is the ionization energy of the active atomic subshell,

$$I_{\mathrm{M}}(E_0, E_1) = a_1(E_0 - E_i^{\mathrm{ion}}) + a_2(E_0 - E_i^{\mathrm{ion}})^2 + a_3(E_0 - E_i^{\mathrm{ion}})^3. \qquad (6)$$

Here we keep the argument E_1 to indicate that the intensity, and hence the parameters a_i, depends on the considered x-ray line. On the other hand the intensity of bremsstrahlung quanta can be expressed as

$$\frac{\mathrm{d}I_{\mathrm{br,M}}(E_0, E_1)}{\mathrm{d}E_1} = Z_{\mathrm{av}}\frac{(E_0 - E_1)}{E_1}$$
$$\times \left[(b_0 + d_0 E_0) + (b_1 + d_1 E_0)\left(\frac{E_1}{E_0}\right) + (b_2 + d_2 E_0)\left(\frac{E_1}{E_0}\right)^2\right], \qquad (7)$$

where Z_{av} is the average atomic number of the material. It is worth mentioning that this expression is a natural generalization of the approximate formula given by Kramers (1923) for the energy distribution of bremsstrahlung photons emitted by electrons of energy E_0,

$$\frac{\mathrm{d}I_{\mathrm{br,M}}^{(\mathrm{Kramers})}(E_0, E_1)}{\mathrm{d}E_1} = b_0 Z_{\mathrm{av}}\frac{(E_0 - E_1)}{E_1}. \qquad (8)$$

Examples of comparisons of Monte Carlo simulation results with the fitted analytical formulae are displayed in figures 1 and 2, which show that differences between the formulae and the simulation results are usually less than the statistical uncertainties of the latter.

It is worth noting that formulae (6) and (7) do account for electron backscattering effects and for the contribution of photons emitted in interactions of fast secondary electrons, which are neglected in the conventional CSDA approach, (4) and (5).

2.2. Absorption of primary x-rays

Not all primary photons that are emitted in the direction of the detector reach the surface of the specimen and the detector. To account for the absorption of primary x-rays on their way to the surface, we need to specify the distribution of emission sites with respect to the depth, z, in the specimen. Note that we set the z-axis parallel to the incoming surface normal (see figure 3) so that points within the specimen have positive z-coordinates.

The depth distribution of x-ray emission sites is given by the $\Phi(\rho z)$ function (Reed 1993), which is proportional to the average number of ionizations produced by primary and fast secondary electrons per unit depth. This function, which is characteristic of each atomic subshell, has been measured experimentally for a limited number of cases (Karduck and Rehback 1991). The most reliable method for computing the $\Phi(\rho z)$ function is Monte Carlo simulation. It is worth recalling that ionizations produced by primary electrons are located at depths of less than the effective electron range, $R_{\mathrm{eff}}(E_0, E_i^{\mathrm{ion}})$, defined as the average path length that electrons with initial

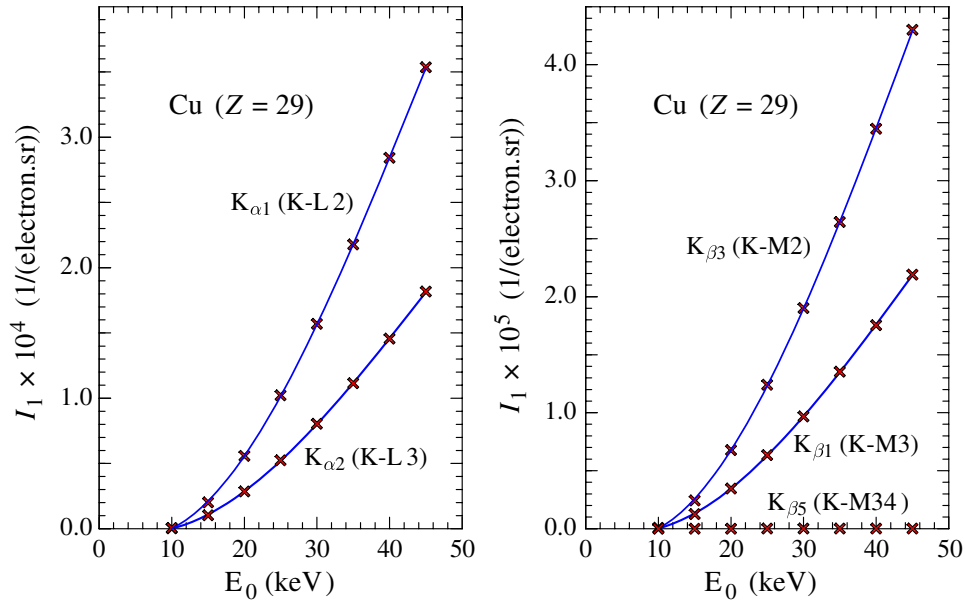J. Phys. D: Appl. Phys. **45** (2012) 225301

X Llovet *et al*

Figure 1. Intensities of the indicated primary x-ray lines of Cu, for an electron beam of energy E_0 impinging normally on a thick sample of Cu. Crosses are results from simulations with PENEPMA; lines represent the analytical approximation (6) with parameters obtained from least-squares fits to the Monte Carlo data.

Figure 2. Bremsstrahlung spectra for electron beams of energy E_0 ranging from 5 to 50 keV impinging normally on a thick sample of Co. Crosses are results from simulations with PENEPMA; lines represent the analytical approximation (7) with parameters obtained from least-squares fits to the Monte Carlo data.
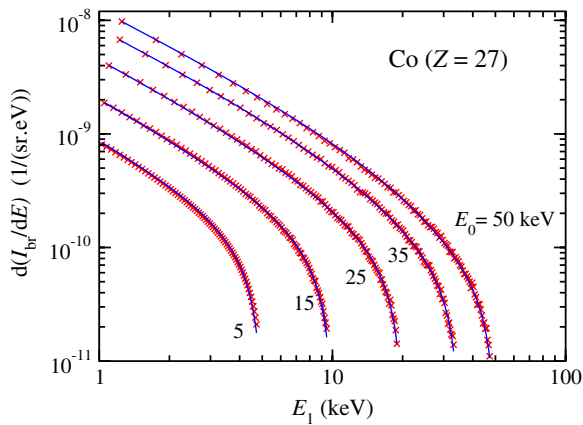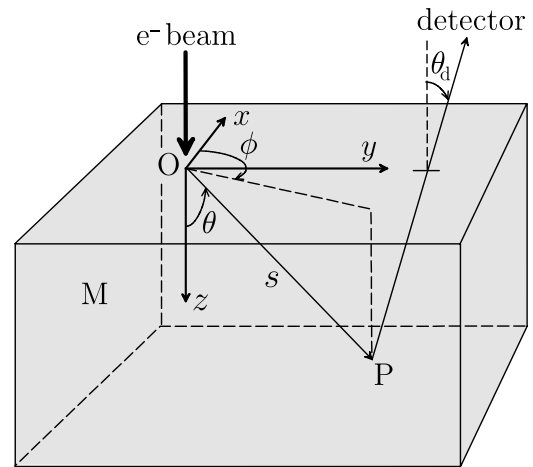

Figure 3. Geometry and reference frame adopted for the calculation of photon intensities from a homogeneous specimen of material M. Primary x-rays of energy E_1 originate from points O near the surface of the specimen, up to depths of the order of the effective range of primary electrons; fluorescent x-rays of energy E_2 may be emitted from much larger depths.

energy E_0 travel before acquiring a kinetic energy equal to the ionization energy E_i^{ion} of the active subshell. Within the CSDA, the effective electron range is given by

$$R_{\text{eff}}(E_0, E_i^{\text{ion}}) = \int_{E_i^{\text{ion}}}^{E_0} \frac{\mathrm{d}E}{S(E)}. \qquad (9)$$

On the other hand, primary bremsstrahlung quanta of energy E are emitted from depths less than about $R_{\text{eff}}(E_0, E)$.

Because we need to give only an approximate account of absorption effects, and because the spatial distribution of x-ray emission sites has only a moderate effect on fluorescence corrections, we shall represent the $\Phi(\rho z)$ function by means of the simple empirical formula proposed by Heinrich (1985),

which can be cast in the form

$$\Phi(\rho z) = \frac{\rho}{a\gamma} \left[\alpha + (1-\alpha)\frac{\rho z}{a\gamma} \right] \exp\left(-\frac{\rho z}{a\gamma}\right), \qquad (10)$$

where ρ is the mass density of the material, in g cm^{-3}, $a = 1.65 \times 10^{-16}$,

$$\gamma = (E_0/\text{keV})^{1.65} - (E_i^{\text{ion}}/\text{keV})^{1.65}, \qquad (11)$$

$$\alpha = 0.18 - \frac{2}{\gamma} + 0.008(E_i^{\text{ion}}/\text{keV}) + 0.005\sqrt{Z_{\text{av}}}, \qquad (12)$$

4

and Z_{av} is the average atomic number of the material. Note that the function (10) is normalized to unity,

$$\int_{-\infty}^{0} \Phi(\rho|z|)\, dz = 1, \tag{13}$$

that is, it can be regarded as the probability density function of the emission depth z of x-rays produced by primary and fast secondary electrons. The calculations that follow can readily be generalized to other, more realistic models of the $\Phi(\rho z)$ function.

The attenuation coefficient of photons of energy E in the material M is

$$\mu_M(E) = \mathcal{N} \sum_a n_a \left[\sigma_{ph}(Z_a, E) + \sigma_{Co}(Z_a, E) \right], \tag{14}$$

where $\sigma_{ph}(Z_a, E)$ and $\sigma_{Co}(Z_a, E)$ are, respectively, the cross sections for photoelectric absorption and Compton scattering by atoms of the element Z_a, and the summation runs over the elements in the material. Each of these cross sections is the sum of contributions from the various electron subshells, i, of the target atom,

$$\sigma_{ph}(Z_a, E) = \sum_i \sigma_{ph,i}(Z_a, E),$$
$$\sigma_{Co}(Z_a, E) = \sum_i \sigma_{Co,i}(Z_a, E), \tag{15}$$

where $\sigma_{ph,i}(Z_a, E)$ and $\sigma_{Co,i}(Z_a, E)$ are the partial cross sections of the ith subshell. Note that $\mu_M(E)$ is the interaction probability of a photon per unit length. Photons are absorbed as they penetrate the material; the probability that a photon reaches a distance s without interacting is given by the familiar exponential attenuation law, $\exp(-\mu_M s)$.

The intensity of primary photons of energy E_1 that reach the detector can now be evaluated as

$$I_M^{det}(E_1) = I_M(E_0, E_1)$$
$$\times \int_0^\infty \Phi(\rho z) \exp\left[-\mu_M(E_1) \frac{z}{\cos\theta_d} \right] dz. \tag{16}$$

The factor in braces describes the effect of absorption. Note that θ_d is the angle between the direction of the detector and the outgoing normal (i.e. the polar angle of the detector direction is $\pi - \theta_d$) and $s = z/\cos\theta_d$ is the path length of a photon within the specimen. In the case of Heinrich's $\Phi(\rho z)$ model (10) the integral can be evaluated analytically, and the result is

$$I_M^{det}(E_1) = I_M(E_0, E_1) \left(\frac{\alpha(\rho/a\gamma)}{\mu_M(E_1)\sec\theta_d + \rho/a\gamma} \right.$$
$$\left. + \frac{(1-\alpha)(\rho/a\gamma)^2}{\left[\mu_M(E_1)\sec\theta_d + \rho/a\gamma \right]^2} \right). \tag{17}$$

2.3. Generation of fluorescent x-rays

Fluorescent quanta (secondary x-rays) are mostly produced by photoelectric absorption of primary photons, although Compton scattering can also give small contributions. Here, for the sake of simplicity, we will only consider x-rays emitted

in the first interaction of primary photons and, accordingly, primary photons are assumed to be effectively absorbed at their first interaction. In reality, Rayleigh and Compton scattering give scattered photons in directions different from those of the primary photons, but the contribution of these scattered photons to the fluorescent signal is small. Secondary x-rays may either leave the specimen or be absorbed. As indicated in the introduction, we have ignored fluorescent quanta emitted through absorption of secondary x-rays.

Let us consider that primary photons of energy E_1 penetrate the material M and generate characteristic x-rays of energy E_2, from transitions that fill a vacancy in the shell j of element Z_b. The number of vacancies in this shell produced per unit path length of a primary photon is

$$V_M(Z_b, j, E_1) = \mu_M(E_1)$$
$$\times \frac{n_b \sum_i \left[\sigma_{ph,i}(Z_b, E_1) + \sigma_{Co,i}(Z_b, E_1) \right] C_{i,j}}{\sum_b n_b \left[\sigma_{ph}(Z_b, E_1) + \sigma_{Co}(Z_b, E_1) \right]}, \tag{18}$$

where the last factor is the probability that the interaction with the primary photon induces a vacancy in subshell j of an atom of the element Z_b, either directly or during relaxation of an initial vacancy in a deeper subshell. The constants $C_{i,j}$ are the probabilities for an initial vacancy in shell i to produce a vacancy in shell j at any stage of the relaxation cascade (Perkins *et al* 1991, Llovet *et al* 2012).

Thus, the intensity of fluorescent x-rays E_2 emitted per unit path length of the primary photon is

$$F_M(E_1, E_2) = \frac{P_{j,2}}{4\pi} V_M(Z_b, j, E_1), \tag{19}$$

where $P_{j,2}$ is the probability that the vacancy in the jth shell migrates to an outer subshell by emission of a photon of energy E_2. Hereafter, quantities pertaining to fluorescent photons will be labelled with the index 2.

All the physical parameters involved in the definitions (14), (18) and (19) can be extracted from the PENELOPE database. The basic approximation in PENELOPE and in the present calculations is that interaction cross sections for atoms bound in molecules and solids can be approximated by those of free atoms (Bragg's additivity approximation). However, modelling of inelastic collisions of electrons does account for binding effects through the use of empirical values of the mean excitation energy, which determines the stopping power of electrons with energies higher than about $0.2\, Z_{av}$ keV. Once the attenuation coefficient $\mu_M(E_1)$ and the fluorescence rate $F_M(E_1, E_2)$ are known, with the aid of the simplifications indicated above, fluorescence corrections for specimens with simple geometries can be readily computed numerically. Consideration of the higher penetration power of photons allows the introduction of a further approximation that permits the analytical evaluation of these corrections for homogeneous specimens and couples.

3. Fluorescence from a homogeneous specimen

We can now formulate the calculation of secondary fluorescence in homogeneous specimens, figure 3. This

J. Phys. D: Appl. Phys. **45** (2012) 225301

X Llovet *et al*

simple geometry is convenient to clarify the approximations employed. Furthermore, calculations for homogeneous samples are needed to obtain the characteristic line intensities in EPMA spectra from standard materials, which determine the so-called *k*-ratios (defined by (39)).

We wish to calculate the intensity of fluorescent x-rays of energy E_2 that reach the detector, i.e. the number of photons per unit solid angle that emerge from the surface in the direction of the detector. We first evaluate the intensity of fluorescent x-rays of energy E_2 released by primary photons of energy E_1, which is given by

$$J^{\mathrm{H}}(E_1, E_2) = 2\pi \, I_{\mathrm{M}}(E_0, E_1) \, F_{\mathrm{M}}(E_1, E_2) \int_0^\infty \mathrm{d}z_0 \, \Phi(\rho z_0)$$
$$\times \left\{ \int_{z_0}^\infty \mathrm{d}z \, \exp\left(-\mu_{\mathrm{M}}(E_2)\frac{z}{\cos\theta_{\mathrm{d}}}\right) \right.$$
$$\times \int_0^1 \frac{\mathrm{d}(\cos\theta)}{\cos\theta} \exp\left(-\mu_{\mathrm{M}}(E_1)\frac{z - z_0}{\cos\theta}\right)$$
$$+ \int_0^{z_0} \mathrm{d}z \, \exp\left(-\mu_{\mathrm{M}}(E_2)\frac{z}{\cos\theta_{\mathrm{d}}}\right)$$
$$\left. \times \int_0^1 \frac{\mathrm{d}(\cos\theta')}{\cos\theta'} \exp\left(-\mu_{\mathrm{M}}(E_1)\frac{z_0 - z}{\cos\theta'}\right) \right\}, \quad (20)$$

where the first exponential in the integrals accounts for the absorption of fluorescent photons along their path to the detector, while the second describes the absorption of primary photons within the specimen. The angle θ' in the second term is the complement to π of the polar angle $\theta' = \pi - \theta$. The integrals are of the type

$$\int_0^1 \frac{\mathrm{d}x}{x} \exp\left(-\frac{a}{x}\right) = \int_a^\infty \frac{\mathrm{d}u}{u} \exp(-u) = \mathcal{E}_1(a), \quad (a > 0),$$
$$(21)$$

where $\mathcal{E}_1(x)$ is the exponential integral (Abramowitz and Stegun 1974). We thus have

$$J^{\mathrm{H}}(E_1, E_2) = 2\pi \, I_{\mathrm{M}}(E_0, E_1) \, F_{\mathrm{M}}(E_1, E_2) \int_0^\infty \mathrm{d}z_0 \, \Phi(\rho z_0)$$
$$\times \left\{ \int_{z_0}^\infty \mathrm{d}z \, \exp\left[-\mu_{\mathrm{M}}(E_2)\sec\theta_{\mathrm{d}}z\right] \mathcal{E}_1\left[\mu_{\mathrm{M}}(E_1)(z - z_0)\right] \right.$$
$$+ \left. \int_0^{z_0} \mathrm{d}z \, \exp\left[-\mu_{\mathrm{M}}(E_2)\sec\theta_{\mathrm{d}}z\right] \mathcal{E}_1\left[\mu_{\mathrm{M}}(E_1)(z_0 - z)\right] \right\}.$$
$$(22)$$

Now, to simplify the calculation, we take advantage of the fact that the effective electron range $R_{\mathrm{eff}}(E_0, E_i^{\mathrm{ion}})$ is much smaller than the photon mean free path $\mu_{\mathrm{M}}^{-1}(E_1)$, typically 10 times smaller or less (Birks *et al* 1966). This implies that $z_0 \mu_{\mathrm{M}}(E) \ll 1$ and the second of the integrals on the right-hand side of (22) is normally much smaller than the first. Consequently, we may assume that primary photons are emitted at the surface of the specimen, i.e. at $z_0 = 0$. The fluorescence correction can then be approximated as

$$J^{\mathrm{H}}(E_1, E_2) \simeq 2\pi \, I_{\mathrm{M}}(E_0, E_1) \, F_{\mathrm{M}}(E_1, E_2)$$
$$\times \int_0^\infty \mathrm{d}z \, \exp\left[-\mu_{\mathrm{M}}(E_2)\sec\theta_{\mathrm{d}}z\right] \mathcal{E}_1\left[\mu_{\mathrm{M}}(E_1)z\right]. \quad (23)$$

The integral over z can be calculated analytically (Abramowitz and Stegun 1974) and gives

$$J^{\mathrm{H}}(E_1, E_2) \simeq 2\pi \, I_{\mathrm{M}}(E_0, E_1) \, F_{\mathrm{M}}(E_1, E_2) \frac{1}{\mu_{\mathrm{M}}(E_2)\sec\theta_{\mathrm{d}}}$$
$$\times \ln\left(1 + \frac{\mu_{\mathrm{M}}(E_2)\sec\theta_{\mathrm{d}}}{\mu_{\mathrm{M}}(E_1)}\right). \quad (24)$$

The characteristic fluorescence E_2 induced by primary characteristic x-rays is obtained by adding the contributions of all x-rays emitted with energies E_j larger than E_2,

$$J_{\mathrm{ch}}^{\mathrm{H}}(E_2) = \sum_j J^{\mathrm{H}}(E_j, E_2) \qquad (E_j > E_2). \quad (25)$$

Similarly, the fluorescence originated from primary bremsstrahlung photons is obtained by integration over the bremsstrahlung energy spectrum given by (7). That is

$$J_{\mathrm{br}}^{\mathrm{H}}(E_2) = \int_{E_2}^{E_0} J^{\mathrm{H}}(E_1, E_2) \frac{\mathrm{d}I_{\mathrm{br,M}}(E_0)}{\mathrm{d}E_1} \, \mathrm{d}E_1. \quad (26)$$

As the integrand is a smooth function of E_1, this integral is well suited for numerical evaluation. We use a simple semi-analytical quadrature method based on log–log linear interpolation on a table with uniformly spaced abscissae. Finally, the total fluorescence intensity in the direction of the detector is

$$J_{\mathrm{M}}^{\mathrm{det}}(E_2) = J_{\mathrm{ch}}^{\mathrm{H}}(E_2) + J_{\mathrm{br}}^{\mathrm{H}}(E_2). \quad (27)$$

4. Fluorescence from a couple

Let us now consider the emission of fluorescent x-rays from a couple consisting of two materials, A and B, separated by a plane interface perpendicular to the surface of the specimen. The electron beam impacts on the left-hand side of the specimen (material A) at a distance d from the interface (figure 4). Primary characteristic photons of energy E_1 from material A can induce emission of fluorescent photons of energy E_2 from materials A and B.

The fluorescence intensity from the right-hand side of the couple (material B) is given by

$$J^{\mathrm{R}}(E_1, E_2) = I_{\mathrm{A}}(E_0, E_1) F_{\mathrm{B}}(E_1, E_2) \int_0^{\pi/2} \mathrm{d}\theta \, \sin\theta \int_0^\pi \mathrm{d}\phi$$
$$\times \int_{d/(\sin\theta \, \sin\phi)}^\infty \mathrm{d}s \, \exp\left(-\mu_{\mathrm{A}}(E_1)\frac{d}{\sin\theta \, \sin\phi} - \mu_{\mathrm{B}}(E_1)\right.$$
$$\times \left. \left(s - \frac{d}{\sin\theta \, \sin\phi}\right) - \mu_{\mathrm{B}}(E_2)\frac{s\cos\theta}{\cos\theta_{\mathrm{d}}}\right), \quad (28)$$

where the first two terms in the argument of the exponential describe the attenuation of primary photons in materials A and B, respectively. The third term accounts for the attenuation of fluorescent x-rays during their flight to the detector. For simplicity, here we assume that detected secondary x-rays only travel through material B, i.e. that the detector is in the right-hand side of the interface, as shown in figure 4. Note that the photon path lengths in materials A and B are

$$s_1 = \frac{d}{\sin\phi \, \sin\theta}, \qquad s_2 = s - s_1 = s - \frac{d}{\sin\phi \, \sin\theta},$$
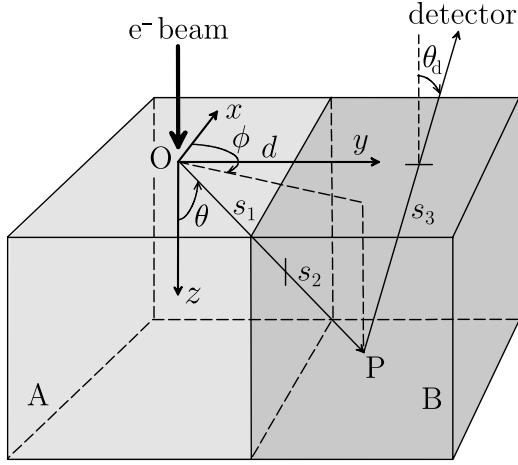$$s_3 = \frac{s\cos\theta}{\cos\theta_{\mathrm{d}}}, \quad (29)$$

Figure 4. Reference frame and geometry adopted in the calculation of fluorescence from a couple with material A on the left of material B. Primary x-rays originate from point O where electrons enter the specimen, at a distance d from the interface. Fluorescent x-rays may be emitted from both materials.

where $s = \overline{\mathrm{OP}}$ is the total path length of the primary photon. The integral over s is analytical and gives

$$J^{\mathrm{R}}(E_1, E_2) = I_{\mathrm{A}}(E_0, E_1) F_{\mathrm{B}}(E_1, E_2) \int_0^{\pi/2} \mathrm{d}\theta$$
$$\times \int_0^{\pi} \mathrm{d}\phi \, \frac{\sin\theta}{\mu_{\mathrm{B}}(E_1) + \mu_{\mathrm{B}}(E_2) \cos\theta \, \sec\theta_{\mathrm{d}}}$$
$$\times \exp\left[-\frac{d}{\sin\theta \, \sin\phi}\left(\mu_{\mathrm{A}}(E_1) + \mu_{\mathrm{B}}(E_2) \cos\theta \, \sec\theta_{\mathrm{d}}\right)\right].$$

Introducing the function

$$G(x) = \int_0^{\pi} \exp(-x/\sin\phi) \, \mathrm{d}\phi, \qquad (30)$$

the intensity $I_2(E_1)$ can be calculated with a single numerical quadrature,

$$J^{\mathrm{R}}(E_1, E_2) = I_{\mathrm{A}}(E_0, E_1) F_{\mathrm{B}}(E_1, E_2)$$
$$\times \int_0^{\pi/2} \mathrm{d}\theta \, \frac{\sin\theta}{\mu_{\mathrm{B}}(E_1) + \mu_{\mathrm{B}}(E_2) \cos\theta \, \sec\theta_{\mathrm{d}}}$$
$$\times G\left(d \, \frac{\mu_{\mathrm{A}}(E_1) + \mu_{\mathrm{B}}(E_2) \cos\theta \, \sec\theta_{\mathrm{d}}}{\sin\theta}\right). \qquad (31)$$

The function $G(x)$ decreases monotonically with x, and has the values $G(0) = \pi$ and $\lim_{x\to\infty} G(x) = 0$. Hence, the fluorescence intensity $J^{\mathrm{R}}(E_1, E_2)$ decreases when the distance d from the electron beam to the interface increases. In the numerical calculations, the function $G(x)$ is evaluated by cubic spline interpolation from a precalculated table. To reduce interpolation errors, the function actually interpolated is $\ln[G(x)]$ for $x \geqslant 0.35$ and $\ln[\pi - G(x)]$ for $x < 0.35$.

The fluorescence intensity from material A (left-hand side of the couple) can be readily evaluated if one assumes that the detector is on the left-hand side of the interface, so that secondary photons reaching the detector do not cross the interface. In this case, the contribution from the region $y < 0$

(on the left of the beam) is

$$J^{\mathrm{L,L}}(E_1, E_2) = I_{\mathrm{A}}(E_0, E_1) F_{\mathrm{A}}(E_1, E_2) \int_0^{\pi/2} \mathrm{d}\theta \, \sin\theta$$
$$\times \int_{\pi}^{2\pi} \mathrm{d}\phi \int_0^{\infty} \mathrm{d}s \exp\left[-\mu_{\mathrm{A}}(E_1) s + \mu_{\mathrm{A}}(E_2) \frac{s \cos\theta}{\cos\theta_{\mathrm{d}}}\right]$$
$$= I_{\mathrm{A}}(E_0, E_1) F_{\mathrm{A}}(E_1, E_2) \pi \, \frac{\cos\theta_{\mathrm{d}}}{\mu_{\mathrm{A}}(E_2)}$$
$$\times \ln\left(1 + \frac{\mu_{\mathrm{A}}(E_2) \sec\theta_{\mathrm{d}}}{\mu_{\mathrm{A}}(E_1)}\right). \qquad (32)$$

Similarly, the intensity of secondary photons generated on the right-hand side of the beam ($0 < y < d$) is

$$J^{\mathrm{L,R}}(E_1, E_2) = I_{\mathrm{A}}(E_0, E_1) F_{\mathrm{A}}(E_1, E_2) \int_0^{\pi/2} \mathrm{d}\theta \, \sin\theta \int_0^{\pi} \mathrm{d}\phi$$
$$\times \int_0^{d/(\sin\theta \sin\phi)} \mathrm{d}s \exp\left[-\mu_{\mathrm{A}}(E_1) s + \mu_{\mathrm{A}}(E_2) \frac{s \cos\theta}{\cos\theta_{\mathrm{d}}}\right]$$
$$= I_{\mathrm{A}}(E_0, E_1) F_{\mathrm{A}}(E_1, E_2)$$
$$\times \int_{\pi/2}^{\pi} \mathrm{d}\theta \, \frac{\sin\theta}{\mu_{\mathrm{A}}(E_1) - \mu_{\mathrm{A}}(E_2) \cos\theta \, \sec\theta_{\mathrm{d}}}$$
$$\times \left[\pi - G\left(d \, \frac{\mu_{\mathrm{A}}(E_1) - \mu_{\mathrm{A}}(E_2) \cos\theta \, \sec\theta_{\mathrm{d}}}{\sin\theta}\right)\right]. \qquad (33)$$

The total fluorescence from material A, $J^{\mathrm{L}} = J^{\mathrm{L,L}} + J^{\mathrm{L,R}}$, is given by

$$J^{\mathrm{L}}(E_1, E_2) = I_{\mathrm{A}}(E_0, E_1) F_{\mathrm{A}}(E_1, E_2) \, 2\pi \, \frac{\cos\theta_{\mathrm{d}}}{\mu_{\mathrm{A}}(E_2)}$$
$$\times \ln\left(1 + \frac{\mu_{\mathrm{A}}(E_2) \sec\theta_{\mathrm{d}}}{\mu_{\mathrm{A}}(E_1)}\right) - I_{\mathrm{A}}(E_0, E_1) F_{\mathrm{A}}(E_1, E_2)$$
$$\times \int_{\pi/2}^{\pi} \mathrm{d}\theta \, \frac{\sin\theta}{\mu_{\mathrm{A}}(E_1) - \mu_{\mathrm{A}}(E_2) \cos\theta \, \sec\theta_{\mathrm{d}}}$$
$$\times G\left(d \, \frac{\mu_{\mathrm{A}}(E_1) - \mu_{\mathrm{A}}(E_2) \cos\theta \, \sec\theta_{\mathrm{d}}}{\sin\theta}\right). \qquad (34)$$

When $d \to \infty$, the second term vanishes, i.e. all fluorescent photons are emitted from material A, and

$$J^{\mathrm{L}}(E_1, E_2) \simeq I_{\mathrm{A}}(E_0, E_1) F_{\mathrm{A}}(E_1, E_2) \, 2\pi \, \frac{\cos\theta_{\mathrm{d}}}{\mu_{\mathrm{A}}(E_2)}$$
$$\times \ln\left(1 + \frac{\mu_{\mathrm{A}}(E_2) \sec\theta_{\mathrm{d}}}{\mu_{\mathrm{A}}(E_1)}\right). \qquad (35)$$

In this limit, the fluorescence intensity is the same as for a thick homogeneous specimen of material A, see (24).

The total fluorescence intensity in the direction of the detector is obtained by adding the contributions from the two materials. That is,

$$J_{\mathrm{AB}}^{\mathrm{det}}(d; E_2) = J_{\mathrm{ch}}^{\mathrm{L}}(E_2) + J_{\mathrm{ch}}^{\mathrm{R}}(E_2) + J_{\mathrm{br}}^{\mathrm{L}}(E_2) + J_{\mathrm{br}}^{\mathrm{R}}(E_2), \quad (36)$$

where

$$J_{\mathrm{ch}}^{\mathrm{L,R}}(E_2) = \sum_j J^{\mathrm{L,R}}(E_j, E_2) \qquad (E_j > E_2), \qquad (37)$$

and

$$J_{\mathrm{br}}^{\mathrm{L,R}} = \int_{E_2}^{E_0} J^{\mathrm{L,R}}(E_1, E_2) \, \frac{\mathrm{d}I_{\mathrm{br,A}}(E_0)}{\mathrm{d}E_1} \, \mathrm{d}E_1 \qquad (38)$$

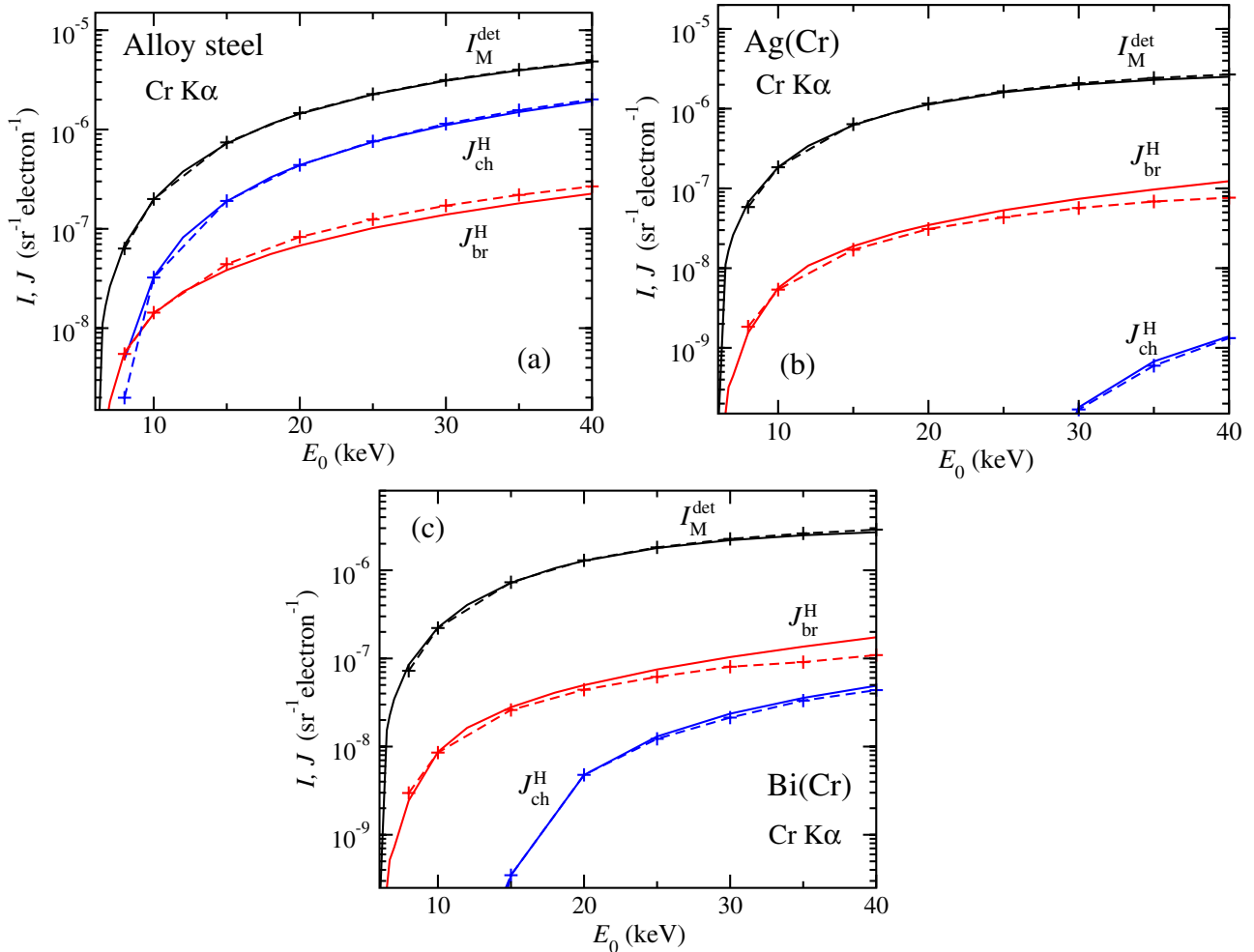are the contributions from primary characteristic photons and bremsstrahlung quanta, respectively.

Figure 5. Primary (I_M^{det}), characteristic fluorescence (J_{ch}^H) and bremsstrahlung fluorescence (J_{br}^H) intensities for Cr Kα x-rays emitted from (*a*) an alloy steel, (*b*) a Ag(Cr) target and (*c*) a Bi(Cr) target as functions of the beam energy (see the text for details). The continuous lines were calculated with the program `fanal`, crosses are results from Monte Carlo simulations with PENEPMA (joined by dashed lines for visual aid).

5. Practical calculations

Fortran programs have been written for the routine calculation of characteristic line intensities of the elements present in a couple and in a homogeneous specimen. The intensities of primary photons are obtained from relatively short runs (less than 60 min) of a modified version of PENEPMA, which describes K-, L- and M-lines. The same program produces extensive tables of photon attenuation coefficients (14) and subshell cross sections for the photoelectric effect and Compton scattering. A second program, named `fitall`, performs the least-squares fits of the simulated intensities of primary photons and gives the parameters of the analytical expressions (6) and (7). All this information is stored in a single parameter file for each material studied. The calculation of the primary intensity of characteristic x-rays, (17), and the fluorescence contributions, (27) and (36), is performed by a standalone program named `fanal`, which reads the parameter files for the materials A and B in the specimen couple and for the standard material M. Atomic relaxation data, needed to determine the fluorescence rates, (18) and (19), are read directly from the PENELOPE database (Perkins *et al* 1991). The program `fanal` delivers the calculated total, primary and fluorescence x-ray intensities

from the specimen, (36) to (38), as well as the intensities from the standard, (25) to (27).

Figure 5 displays a comparison between calculated and simulated characteristic and bremsstrahlung fluorescence intensities for Cr Kα photons emitted from three homogeneous specimens. These are an alloy steel (composition Si 0.26 wt%, Cr 1.16 wt%, Mn 0.47 wt%, Fe 96.44 wt%, Ni 0.10 wt% and Mo 1.42 wt%), a Ag(Cr) target (Ag 99 wt% and Cr 1 wt%) and a Bi(Cr) target (Bi 99 wt% and Cr 1 wt%). For the sake of completeness, the corresponding primary Cr Kα x-ray intensities are also displayed. Agreement between calculated and simulated primary and characteristic fluorescence intensities is remarkable. This is because characteristic fluorescent x-rays are emitted isotropically, as assumed in the calculations. In the case of bremsstrahlung fluorescence, however, the calculations from `fanal` depart somewhat from simulation results, especially at high beam energies. Most of the differences are caused by our simplifying assumption that bremsstrahlung photons are emitted isotropically. As indicated above, this assumption does not hold for the high-energy tip of the photon spectrum because photons with energies close to the beam energy E_0 are emitted by electrons that have travelled a small path length

within the sample and, consequently, move in directions close to that of the incident beam. Unfortunately, it does not seem possible to account for the correlation between the energy and the direction of emission of bremsstrahlung photons without considerably increasing the complexity of the calculations.

EPMA measurements performed on material couples have generally reported the so-called *k*-ratio, which is defined for a characteristic line of element Z_a composing the A–B couple, identified by the photon energy E_2, as

$$k = \frac{I_A^{det}(E_2) + J_{AB}^{det}(d; E_2)}{I_M^{det}(E_2) + J_M^{det}(E_2)}, \qquad (39)$$

where $I_A^{det}(E_2)$ is the primary fluorescence intensity of the measured line on material A (17) and $J_{AB}^{det}(d; E_2)$ is the total fluorescence intensity of the measured line on the A–B couple when the electron beam impacts on material A at a distance d from the interface (36). $I_M^{det}(E_2)$ and $J_M^{det}(E_2)$ are the primary and total fluorescence intensities, respectively, of the same line measured on a homogeneous sample (a standard) of material M, under equivalent experimental conditions ((17) and (27)). In the measurements and calculations presented below, material M is the pure element Z_a, because this election simplifies quantitative analysis (see, e.g., Reed 1993). It is pertinent to mention that, for a bulk sample of material A, $J_{AB}^{det}(d; E_2)$ reduces to $J_A^{det}(E_2)$, and then $k \times 100$ gives approximately the concentration c_a (in %) of element Z_a (Reed 1993). In the case of measurements on a couple A–B such that the active element Z_a is present only in material B, with the electron beam impinging on material A at a distance d from the interface, $I_A^{det}(E_2) = 0$ and $k \times 100$ can be interpreted as the approximate 'apparent' concentration of element Z_a in material A due to fluorescence from material B.

6. Results and discussion

In order to assess the reliability of the proposed semi-analytical calculation method and that of PENELOPE, we have compared calculated fluorescence intensities with results from PENELOPE simulations and with data from EPMA measurements on material couples taken from the literature. The selected measurements pertain to metal–metal (Bastin *et al* 1983, Valovirta *et al* 2001), alloy–alloy (Bastin *et al* 1983) and mineral–mineral (Dalton and Lane 1996, Wark and Watson 2006) couples. In this kind of experiment, the samples are generally prepared by cold-pressing the two involved materials together after they have been both ground and polished in order to obtain a sharp interface when joined together. The assembly is subsequently sectioned and polished. For the selected experiments, the energies of the electron beam range from 15 to 20 keV (as indicated in the figures). In general, primary characteristic photons of energy E_1 from material A may induce emission of fluorescent photons of energy E_2 from both materials A and B. In some cases considered below, the fluorescence photons are generated only through the interaction of bremsstrahlung photons, while in other cases, the fluorescence has contributions from both characteristic and bremsstrahlung photons.

It should be noted that our semi-analytical calculation scheme (as well as our Monte Carlo simulations) introduce two simplifying assumptions, which depend on the orientation of the specimen with respect to the spectrometer and may affect comparison with experimental data. Firstly, as discussed above, we have assumed that the detected secondary x-rays only travel through the material where they are produced. Thus, in the case of couples, the line intensities for x-ray photons from material B are calculated by considering that the detector is on the right-hand side of the interface (see figure 4). Unfortunately, there is no guarantee that experiments meet this requirement, because the orientation of the specimen with respect to the x-ray detector is generally not given in descriptions of EPMA measurements (the work of Dalton and Lane (1996), is one of the few exceptions known to the authors). In the case that the detector is placed on the left-hand side of the interface, fluorescence x-rays will also travel within material A in their way to the detector, with attenuation coefficient μ_A. Thus if $\mu_A < \mu_B$, an increase in the detected x-ray intensity is to be expected. The second simplifying assumption is that all x-rays emerging from the surface of the specimen in the direction of the detector are assumed to be recorded, regardless of the position from where they are emitted, which may be as much as several tens of micrometres from the point of impact of the electron beam. This is not the case for measurements performed with wavelength-dispersive spectrometers, which have a maximum focusing efficiency only for photons emitted from the Rowland circle of the spectrometer (Reed 1993). As discussed by Dalton and Lane (1996), the loss of efficiency (or degree of defocusing) may be significant for x-rays generated along the spectrometer direction, even a short distance from the Rowland circle, but it is negligible for those x-rays generated along a line perpendicular to the spectrometer direction. Note that the sample orientation for which spectrometer defocusing is minimal (interface along the direction of the spectrometer) satisfies the condition that the detector is on the right-hand side of the interface.

The Monte Carlo simulations reported here were performed with PENELOPE using the main program PENEPMA (Pinard *et al* 2012). As mentioned above, this program implements the variance-reduction technique of interaction forcing an increase of the efficiency of x-ray generation. The emerging x-rays were tallied using an annular detector, which covers the solid angle corresponding to $(\theta_d - 5^o, \theta_d + 5^o)$. The use of this annular detector represents a very effective improvement in the efficiency of the simulation, although it is only justified when the emerging x-ray flux is axially symmetric. This introduces geometrical modifications similar to those implicit in the semi-analytical calculations.

Figure 6(*a*) displays calculated, simulated and measured Co Kα *k*-ratios as functions of the distance of the electron beam to the interface for a Cu–Co couple, when the beam impacts on the Cu side of the couple. The opposite case is illustrated in figure 6(*b*), which shows the distance-dependent Cu Kα *k*-ratio obtained when the beam impinges on the Co side of the Cu–Co couple. The measurements were performed by Bastin *et al* (1983). It is worth noting that when the electron beam impinges on Cu (the element of highest atomic number), Cu characteristic x-rays are able to ionize the Co atoms, and
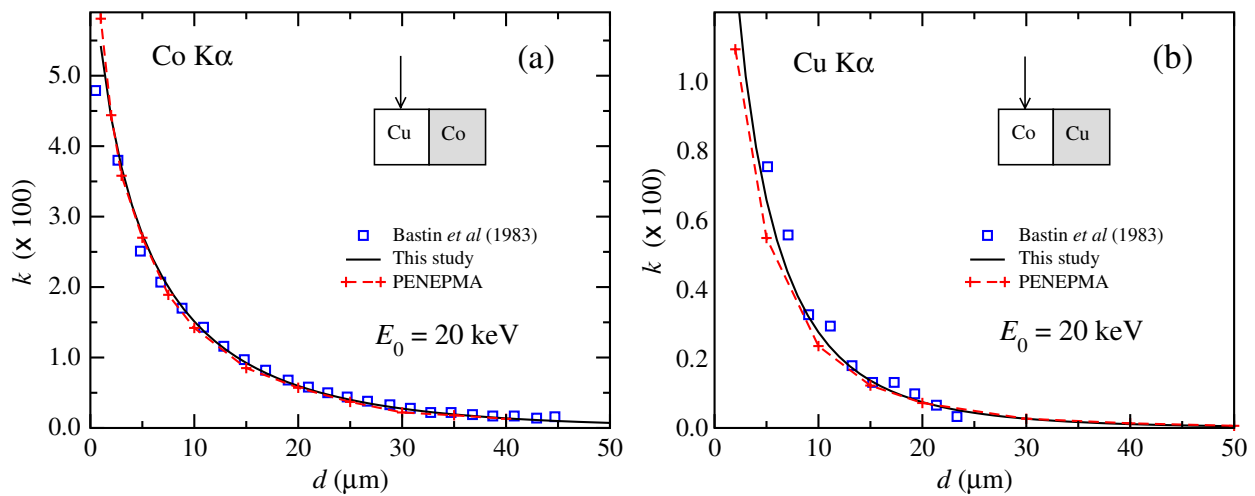
Figure 6. Comparison of measured, calculated and simulated Co (*a*) and Cu (*b*) Kα k-ratios versus electron beam distance *d* to the interface for a Co–Cu couple and electrons impinging on the Cu (*a*) and Co (*b*) sides of the couple. The measured, calculated and simulated values are represented by open squares, continuous lines and crosses (joined by dashed lines for visual aid), respectively.
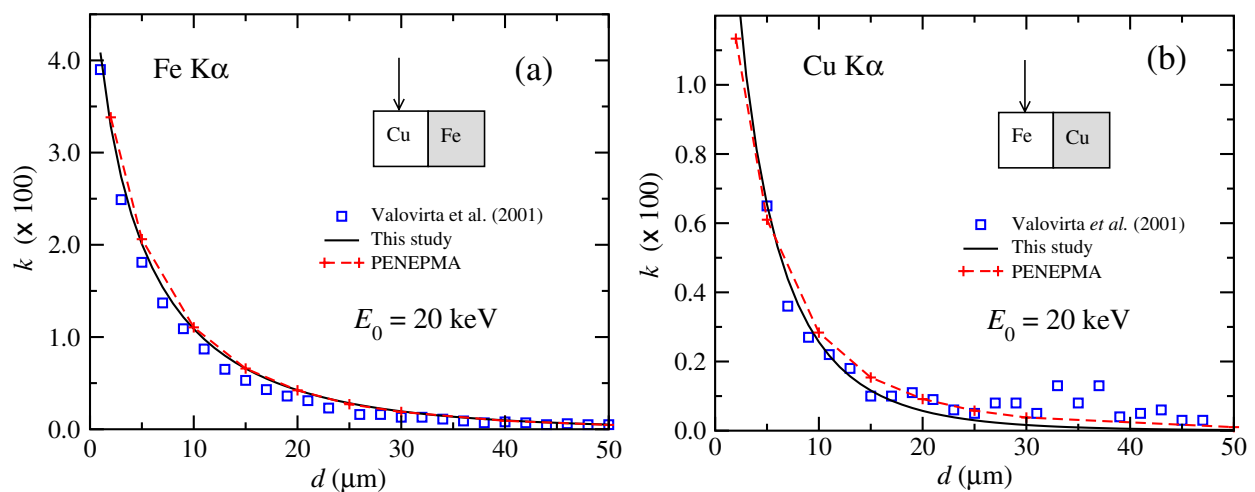

Figure 7. Comparison of measured, calculated and simulated Fe (*a*) and Cu (*b*) Kα k-ratios versus electron beam distance *d* to the interface for a Fe–Cu couple and electrons impinging on the Cu (*a*) and Fe (*b*) sides of the couple. The measured, calculated and simulated values are represented by open squares, continuous lines and crosses (joined by dashed lines for visual aid), respectively.

therefore, the observed Co *k*-ratio is due to the contributions of both characteristic x-rays and bremsstrahlung. Conversely, when the beam impacts on the Co side of the specimen (the element of lowest atomic number), there is no characteristic contribution to the fluorescence intensity of Cu Kα, which is only due to the interaction of bremsstrahlung photons. In both cases, the agreement between calculated, simulated and measured *k*-ratios is remarkably good. It is interesting to note that the observed differences between simulated and calculated bremsstrahlung fluorescence intensities, see figure 5, have a lesser effect on the *k*-ratios, because of a partial cancellation of common factors in the intensities from the specimen and from the standard. A similar comparison is illustrated in figure 7, for a Fe–Cu couple. In this case, the experimental data were measured by Valovirta *et al* (2001). Agreement between simulated, calculated and measured *k*-ratios is, in general, satisfactory, although it is not as good as in the case of the Co–Cu couple. Both simulated and calculated *k*-ratios seem to be slightly higher than the measurement values when the

beam impacts on the Cu side of the couple, and the calculated *k*-ratios are somewhat lower than the simulation results when the beam impacts on the Fe side of the couple.

Figure 8 compares calculated, simulated and measured *k*-ratio profiles for couples consisting of a homogeneous Cu(Co) alloy and a Co (4.1 wt% Cu) alloy as functions of the distance from the beam to the boundary. These kinds of alloy couples are typical starting materials for diffusion experiments using the diffusion couple technique (Kodentsov *et al* 2001). Two different Cu(Co) alloys, Cu (4.1 wt% Co) and Cu (2.4 wt% Co), are considered, with the beam impacting on the Cu(Co) alloy in both cases. The experimental data were measured by Bastin *et al* (1983). For the two specimens, the measured Co Kα x-ray intensity has a primary contribution (from electron impact on the Cu(Co) alloy itself) and a contribution from secondary fluorescence due to the interaction of Co characteristic x-rays and bremsstrahlung within the Co(Cu) alloy. In the case of the Cu (2.1 wt% Co) alloy, simulated, calculated and measured fluorescence intensities agree well,
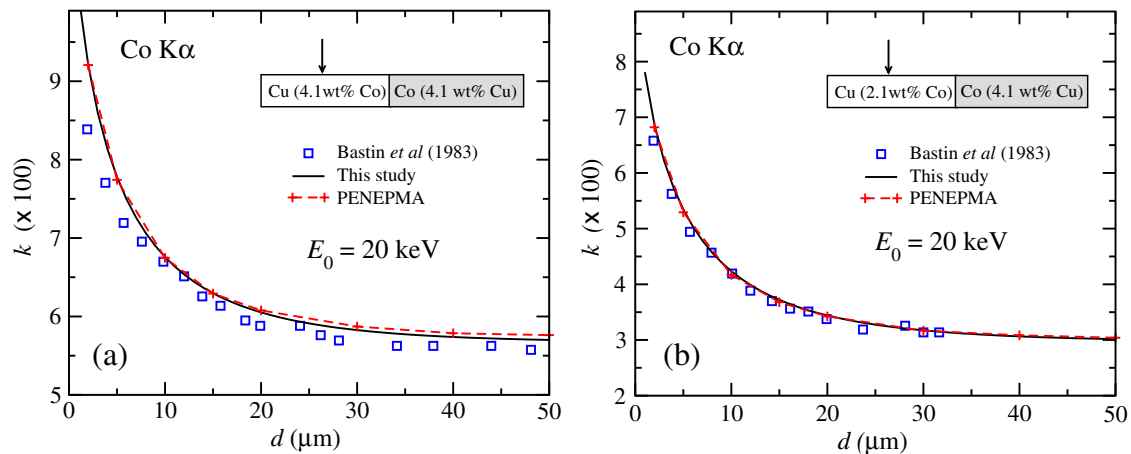
Figure 8. Comparison of measured, calculated and simulated Co Kα *k*-ratios versus electron beam distance *d* to the interface for a Cu (4.1 wt% Co)–Co (4.1 wt%) couple (*a*) and in a Cu (2.4 wt% Co)–Co (4.1 wt%) couple. The beam impacts on the Cu(Co) alloys. The measured, calculated and simulated values are represented by open squares, continuous lines and crosses (joined by dashed lines for visual aid), respectively.

while for the Cu (4.2 wt% Co) sample, both simulated and calculated intensities also agree well, but they give *k*-ratios that are somewhat larger than experimental data. These differences could be partially attributed to uncertainties in the geometrical orientation of the sample, as discussed earlier.

Shown in figure 9 is a comparison of calculated, simulated and measured *k*-ratios for Ti Kα x-rays emitted from a SiO$_2$–TiO$_2$ couple, as a function of distance of the electron beam to the boundary. The measurement of Ti in this mineral couple is widely used for the purpose of determining the temperature at which the minerals were formed (geothermometer). The measurements were performed by Wark and Watson (2006), who developed and calibrated this geothermometer. Note that the fluorescent Ti x-rays are caused only by the interaction of bremsstrahlung photons in the TiO$_2$ phase. Even when the electron beam impacts at a distance of 100 μm from the TiO$_2$ phase, the fluorescence contribution yields an apparent Ti concentration of ~100 ppm, which will result in sizeable temperature overestimations. Both calculation and simulation results are seen to agree well with measurements.

Up to now, we have focused our comparison on single- or two-element materials. Apart from some minor differences, the agreement between calculation, simulation, and experiment was found to be fairly good. The next comparison concerns the same kind of test but performed on multi-component materials, namely couples of different olivine minerals (i.e. a magnesium iron silicate with the formula (Mg,Fe)$_2$SiO$_4$) in contact with diopside (i.e. a silicate of the pyroxene group with the formula MgCaSi$_2$O$_6$). The considered olivine samples are identified by their content of the solid-solution end-member forsterite (Fo) (the lower the forsterite content, the higher the Fe concentration). The experimental measurements were performed by Dalton and Lane (1996). Figure 10 compares calculated, simulated and measured *k*-ratios for Ca Kα x-rays for the olivine–diopside couples under consideration, as functions of the distance from the electron beam to the boundary, with the electron beam impinging on the olivine phase. In this case, the secondary fluorescent Ca Kα x-rays originate essentially
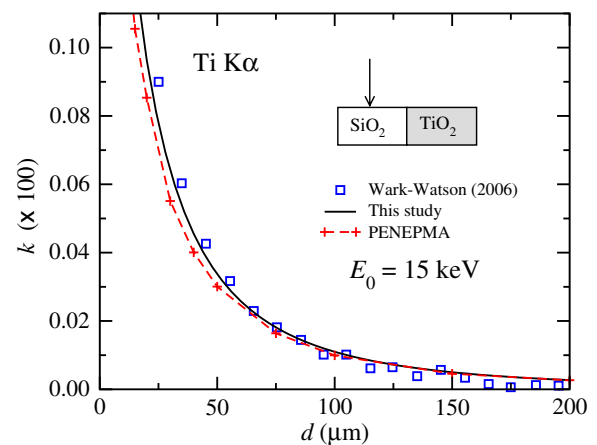

Figure 9. Comparison of measured, calculated and simulated Ti Kα *k*-ratio versus electron beam distance *d* to the interface for a SiO$_2$–TiO$_2$ couple and electron beams impacting on the SiO$_2$ side of the couple. The measured, calculated and simulated values are represented by open squares, continuous lines and crosses (joined by dashed lines for visual aid), respectively.

from the interaction in diopside of Fe Kα x-rays as well as bremsstrahlung photons. In spite of the larger experimental uncertainties, the comparison shows reasonable agreement between calculations, simulations and measurements.

In conclusion, we have shown that the results of Monte Carlo simulations of secondary fluorescence with PENELOPE using the dedicated code PENEPMA give very good agreement with EPMA experiments for a wide variety of material couples. This gives us confidence in using the physical interaction models implemented in PENELOPE in our semi-analytical calculations. We have also shown that secondary fluorescence intensities calculated by means of the proposed semi-analytical method agree well with both Monte Carlo simulations results and experimental data. The application of the developed code for correcting on-line EPMA analyses should be straightforward (see, e.g., Bastin *et al* 1983). Work along these lines is currently in progress. The developed code is publicly available from the authors.
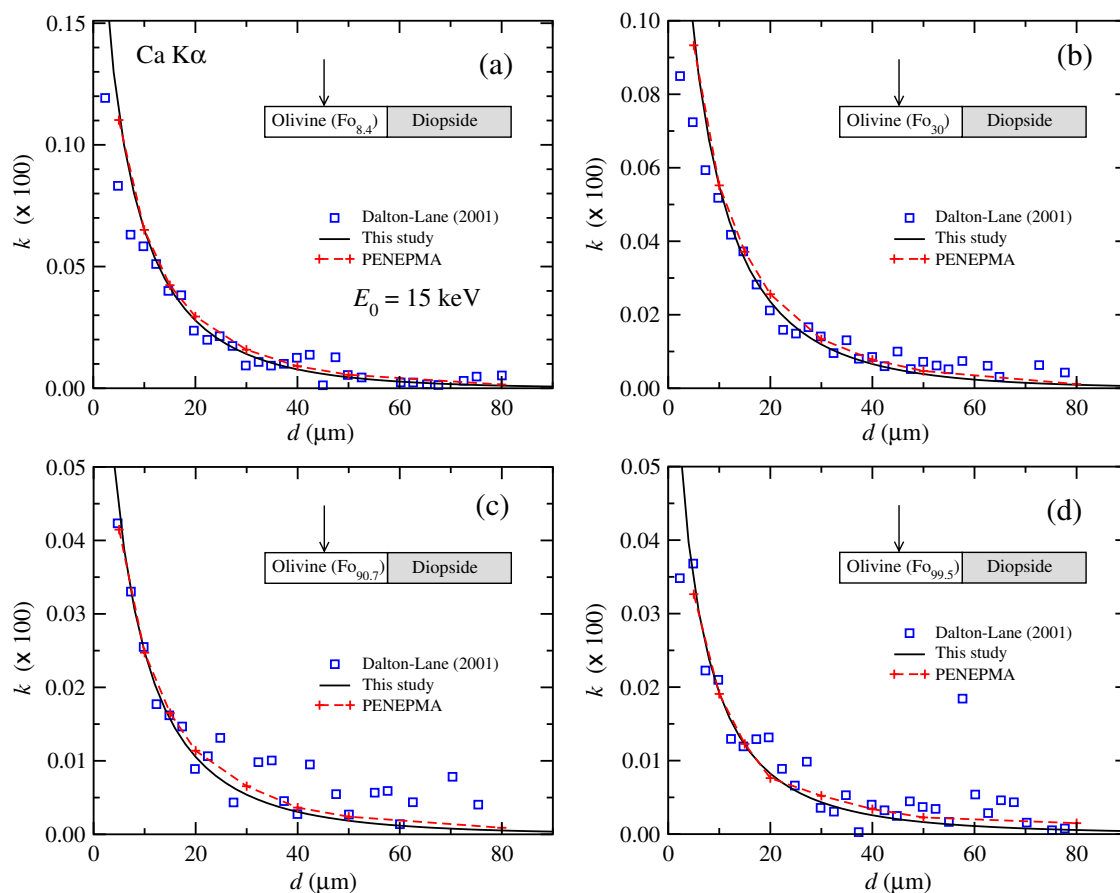
Figure 10. Comparison of measured, calculated and simulated Ca Kα k-ratio versus electron beam distance d to the interface, for couples of olivine with 8.4% (*a*), 30% (*b*), 90% (*c*) and 99% (*d*) of Forsterite contents in contact with diopside, and electron beams impacting on the olivine side of the couples. The measured, calculated and simulated values are represented by open squares, continuous lines and crosses (joined with by dashed lines for visual aid), respectively.

Acknowledgments

References

Abramowitz M and Stegun I A 1974 *Handbook of Mathematical Functions, With Formulas, Graphs, and Mathematical Tables* (Dover: New York)
Birks L S, Ellis D J, Grant K, Frisch A S and Hickman R B 1966 *The Electron Microprobe* ed T D McKinley *et al* (New York: Wiley) p 199
Bastin G F, van Loo F J, Vosters P J, Vroljik J W 1983 *Scanning* **5** 172
Cox M G C, Love G and Scott V D 1979 *J. Phys. D: Appl. Phys.* **12** 1441
Dalton J A and Lane S J 1996 *Am. Mineral.* **81** 194
Escuder J A, Salvat F, Llovet X, Donovan J J 2010 *IOP Conf. Ser.: Mater. Sci. Eng.* **7** 012008
Fournelle J H, Kim S and Perepezko J H 2005 *Surf. Interface Anal.* **37** 1012
Heinrich K F J 1985 *Microbeam Analysis* ed J T Armstrong (San Francisco, CA: San Francisco Press) p 79
Hénoc J, Heinrich K F J and Zemskoff A 1969 *5th Int. Congress on X-ray Optics and Microanalysis* ed G Möllenstedt and K H Gaukler (Springer: Berlin) p 187

Karduck P and Rehback W 1991 *Electron Probe Quantitation* ed K F J Heinrich and D E Newbury (New York: Plenum) p 191
Kramers H A 1923 *Phil. Mag.* **46** 836
Kodentsov A A, Bastin G F and van Loo F J J 2001 *J. Alloys Compounds* **320** 207
Llovet X and Galan G 2003 *Am. Mineral.* **88** 121
Llovet X, Fernandez-Varea J M, Sempau J and Salvat F 2005 *Surf. Interface Anal.* **37** 1054
Llovet X, Powell C J, Salvat F and Jablonski A 2012 submitted
Maurice F, Seguin R and Hénoc J 1965 *Optique de Rayons X et Microanalyse* ed R Castaing *et al* (Paris: Hermann) p 357
Perkins S T, Cullen D E, Chen M H, Hubbell J H, Rathkopf J and Scofield J 1991 *Report UCRL-50400* vol 30 (Lawrence Livermore National Laboratory: Livermore)
Pinard P T, Hendrix D, Llovet X, Gauvin R and Salvat F 2012 submitted
Reed S J B 1965 *Brit. J. Appl. Phys.* **16** 913
Reed S J B and Long J V P 1963 *X-ray Optics and X-ray microanalysis* ed H H Patee *et al* (New York: Academic) p 317
Reed S J B 1993 *Electron Microprobe Analysis* (Cambridge: Cambridge University Press)
Salvat F, Fernández-Varea J M and Sempau J 2011 PENELOPE-2011: A code system for Monte Carlo simulation of electron and photon transport (OECD/NEA Data Bank: Issy-les-Moulineaux, France)
Valovirta E, Erlach S, Llovet X, Heikinheimo E 2001 *Proc. EMAS 2001* p 382
Wark D A and Watson E B 2006 *Contrib. Mineral. Petrol.* **152** 743
Youhua H, Yencai H and Jianguang C 1988 *J. Phys. D: Appl. Phys.* **21** 1221